Efficient Assessment of the Instantaneous Power Distributions of Pulse-Shaped Single- and Multi-Carrier Signals

Sebastian Stern and Robert F.H. Fischer
Institut für Nachrichtentechnik, Universität Ulm, Ulm, Germany, Email: {sebastian.stern, robert.fischer}@uni-ulm.de

***Abstract*—We present a new approach for assessing the instantaneous power distributions of the continuous-time transmit signal (i.e., after pulse shaping) in single- and multi-carrier transmission schemes. On the one hand, an efficient calculation of the distribution for single-carrier signals via the fast Fourier transform (FFT) is given. On the other hand, tight approximations for multi-carrier transmission based on orthogonal frequency-division multiplexing (OFDM) are reviewed. Thereby, the effect of non-modulated carriers (guard bands) is taken into account. The impact of the roll-off factor of root-raised-cosine pulse shaping is analyzed and its converse influence on the peak-to-average power behavior of both modulation strategies is discussed. All theoretical derivations match very well with numerical results obtained from Monte–Carlo simulations.**

I. Introduction

The peak-to-average power ratio (PAR) behavior of a modulation scheme is an important parameter in the design of digital communication systems, since the PAR significantly affects the implementation of the power amplifier in the radio frontend. Consequently, an efficient and accurate assessment of different modulation formats is highly desirable. In particular, the statistical properties of the *instantaneous power* (squared envelope) of the transmit signal are of interest.

Unfortunately, up to now, no final solutions to the problem at hand have been presented in the literature. In case of single-carrier modulation employing amplitude shift-keying (ASK) or quadrature-amplitude modulation (QAM) signal constellations, only upper and lower bounds on the distribution of the instantaneous power were known [12], [13]. Besides this, theoretical considerations on the maximum possible PAR were carried out in [2]. Recently, an approach that enables a precise calculation of the distribution of instantaneous power for QAM was proposed [7], however, at the cost of high computational complexity.

For multi-carrier modulation schemes, particularly orthogonal frequency-division multiplexing (OFDM), tight approximations for the PAR behavior already exist for a long time (e.g., [5], [6], [14]). However, in these publications, either the behavior of the discrete-time transmit symbols is studied, or that of the continuous-time signal assuming ideal low-pass filtering. Both cases are not suited for performing a fair comparison with single-carrier transmissions. Consequently, we present a new approach for an efficient assessment of the instantaneous power distribution for single- and multi-carrier schemes. Based thereon, a meaningful comparison and discussion on the different behaviors is possible.

The paper is organized as follows: First, in Section II, we describe the theoretical derivation of the PAR statistics for ASK and QAM signaling and give an efficient numerical implementation. The usual, well-suited approximation for OFDM is reviewed in Section III. The effect of oversampling, usually employed in practice, is discussed from the PAR perspective. Finally, in Section IV, a comparison of the different statistical properties of single- and multi-carrier signals is drawn. The paper closes with a brief conclusion (Section V).

II. Single-carrier signals

A. System Model

In this paper, we consider single-carrier pulse-amplitude modulation (PAM). The block diagram of the transmitter is depicted in Fig. 1. First, the redundancy-free sequence of binary

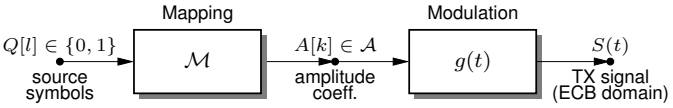

Fig. 1. Transmitter model of single-carrier PAM transmission.

source symbols $Q[l] \in \{0,1\}$ (bits) is mapped to amplitude coefficients of a given signal constellation $\mathcal{A}$ with cardinality $M = |\mathcal{A}|$. By this, we obtain a sequence of independent and identically distributed random variables[1] $A[k]$, $k \in \mathbb{Z}$. Then, the transmit signal in the equivalent complex baseband (ECB) [3], [9] is formed via

$$S(t) = \sum\nolimits_{k=-\infty}^{\infty} A[k]\, g(t - kT)\ , \tag{1}$$

where T is the symbol interval and $g(t)$ denotes the impulse response of transmit filer (i.e., basic pulse shape).

We examine two possible choices of the signal constellation: In the case of bipolar ASK, we restrict to real-valued random variables $A[k] \in \mathbb{R}$, drawn from the constellation

$$\mathcal{A}_{\mathrm{ASK}} \stackrel{\mathrm{def}}{=} \big\{ c \cdot \underbrace{(2m - (M+1))}_{a_m} \ \big|\ m \in \{1, 2, \ldots, M\} \big\}\ . \tag{2}$$

When employing square QAM constellations (i.e., $\sqrt{M} \in \mathbb{N}$), we have $A[k] = A_{\mathrm{I}}[k] + \mathrm{j}\, A_{\mathrm{Q}}[k]$, where $\mathcal{A}_{\mathrm{I}} = \mathcal{A}_{\mathrm{Q}} = \mathcal{A}_{\mathrm{ASK}} = \{a_1, a_2, \ldots, a_{\sqrt{M}}\}$. The normalization constants are set to $c_{\mathrm{ASK}} = 1/\sqrt{(M^2-1)/3}$ and $c_{\mathrm{QAM}} = 1/\sqrt{2(M-1)/3}$, respectively, leading to $\sigma_A^2 \stackrel{\mathrm{def}}{=} \mathrm{E}\{|A[k]|^2\} = 1$. As we assume a redundancy-free sequence of source symbols, the amplitude coefficients are uniformly distributed with probability $1/M$.

[1] Notation: Random variables are typeset in capitals, realizations thereof in lowercase letters. $\mathrm{E}\{\cdot\}$ denotes expectation; $\mathrm{si}(x) \stackrel{\mathrm{def}}{=} \frac{\sin(x)}{x}$ is the sinc function. $\inf\{\cdot\}$ denotes the infimum operator.

Throughout the paper, we consider a real-valued square-root raised-cosine (RRC) pulse-shaping filter $g(t)$ with some roll-off factor $\alpha \in [0,1]$ and energy E_g [9, p. 675]. This choice, together with the receiver-side matched filter, guarantees inter-symbol interference-free detection instances. In practice, the impulse response has to be limited to a finite length[2] $L = KT$, i.e., $g(t) = 0$, $\forall t \notin \left[-\frac{K}{2}T, \frac{K}{2}T\right)$, with $K \in \mathbb{N}$ and K even.

Since the ECB transmit signal $S(t)$ is a cyclostationary random process [4] its statistical characteristics vary periodically over time with period T. Consequently, w.l.o.g., we can restrict the assessment to the interval $t \in [0,T)$. Similar to the procedure in [7], [12], we substitute the random variables in (1) by new random variables $A_\kappa \stackrel{\text{def}}{=} A[\kappa - K/2]$ and the filter coefficients by $g_\kappa(t) \stackrel{\text{def}}{=} g(t - (\kappa - K/2)T)$ with new index $\kappa \in \{1, 2, \ldots, K\}$. As a result, we obtain

$$S(t) = \sum\nolimits_{\kappa=1}^{K} g_\kappa(t) A_\kappa \ , \quad t \in [0,T) \ . \tag{3}$$

From (3), we see that the ECB signal's value at a certain time instant is given by the addition of products

$$S_\kappa(t) \stackrel{\text{def}}{=} g_\kappa(t) A_\kappa \ , \tag{4}$$

i.e., $S(t)$ is the sum of random amplitude coefficients, each weighted by a filter coefficient, dependent on the observation time.

B. Statistical Description of Instantaneous Power

We are interested in assessing the statistical distributions of the instantaneous power (IP) $P(t) \stackrel{\text{def}}{=} |S(t)|^2$. It is convenient to normalize this quantity to the average power. Since we have $\sigma_A^2 = 1$, the *normalized instantaneous power* is given as

$$P_\mathrm{n}(t) \stackrel{\text{def}}{=} \frac{P(t)}{E_\mathrm{g}/T} \ . \tag{5}$$

The complementary cumulative distribution function (ccdf)

$$\mathit{\Gamma}_{P_\mathrm{n}(t)}(p_\mathrm{n}) \stackrel{\text{def}}{=} \Pr\{P_\mathrm{n}(t) \geq p_\mathrm{n}\} = 1 - F_{P_\mathrm{n}(t)}(p_\mathrm{n}) \ , \tag{6}$$

where $F_{P_\mathrm{n}(t)}(p_\mathrm{n})$ is the cumulative distribution function (cdf), is well-suited for characterizing the occurrence of large instantaneous powers.

The cyclostationarity of the process $P_\mathrm{n}(t)$ is usually taken into account by considering *time-averaged distributions*, specifically, the average ccdf[3]

$$\mathit{\Gamma}_{\bar{P}_\mathrm{n}}(p_\mathrm{n}) = \frac{1}{T} \int_0^T \mathit{\Gamma}_{P_\mathrm{n}(t)}(p_\mathrm{n}) \, \mathrm{d}t \ . \tag{7}$$

As we want to assess the PAR behavior of different modulation formats, our goal is to obtain the particular values of the IP that are exceeded with a certain probability $\psi \in [0,1]$, e.g., $\psi = 10^{-5}$. It is well-known, that such an approach is much more relevant than considering the maximum possible values. Hence, we study the *inverse ccdf* (iccdf)

$$\mathit{\Gamma}^{-1}_{\bar{P}_\mathrm{n}}(\psi) \stackrel{\text{def}}{=} \inf\{p_\mathrm{n} \in \mathbb{R}_0^+ \mid \mathit{\Gamma}_{\bar{P}_\mathrm{n}}(p_\mathrm{n}) \leq \psi\} \ . \tag{8}$$

C. Efficient Assessment of Distributions for ASK

In this section, we present a strategy based on characteristic functions which enables an exact computation of the IP distribution. In contrast to the approach in [7], where characteristic functions using polar coordinates are applied, we resort to Cartesian coordinates.

The characteristic function of a random variable X is the (inverse) Fourier transform of the probability density function (pdf) $f_X(x)$ [8]

$$\varphi_X(\omega) \stackrel{\text{def}}{=} \mathrm{E}\{\mathrm{e}^{\mathrm{j}\omega X}\} = \int_{-\infty}^{\infty} f_X(x) \cdot \mathrm{e}^{\mathrm{j}\omega x} \, \mathrm{d}x \ . \tag{9}$$

For uniform M-ary ASK, the characteristic function is readily determined as

$$\varphi_{S_\kappa(t)}(\omega) = \frac{2}{M} \sum\nolimits_{m=1}^{M/2} \cos(\omega g_\kappa(t) a_m c_\mathrm{ASK}) \ . \tag{10}$$

In case of $M \to \infty$, the coefficients are uniformly distributed within the interval $[-\sqrt{3}, \sqrt{3}]$ [12], and the characteristic function is given as

$$\varphi_{S_\kappa(t)}(\omega) = \mathrm{si}(\omega g_\kappa(t) \sqrt{3}) \ . \tag{11}$$

Since the addition of independent random variables results in the multiplication of their characteristic functions [8], we obtain the characteristic function of $S(t)$ as

$$\varphi_{S(t)}(\omega) = \prod\nolimits_{\kappa=1}^{K} \varphi_{S_\kappa(t)}(\omega) \ . \tag{12}$$

Because the Fourier transform of $\varphi_{S(t)}(\omega)$ yields the corresponding pdf $f_{S(t)}(s)$, the requested ccdf calculates to

$$\mathit{\Gamma}_{S(t)}(s) = \int_s^{\infty} f_{S(t)}(\xi) \, \mathrm{d}\xi \ . \tag{13}$$

Finally, using the symmetry of bipolar ASK, the ccdf of normalized IP results from $\mathit{\Gamma}_{P_\mathrm{n}(t)}(p_\mathrm{n}) = 2\,\mathit{\Gamma}_{S(t)}(\sqrt{p_\mathrm{n}(E_\mathrm{g}/T)})$.

The main advantage of this (analytically correct) approach is the feasibility of an efficient numerical implementation employing a fast Fourier transform (FFT). After calculating the characteristic functions (10) and (12), one single FFT operation is sufficient to obtain (a sampled version of) the pdf $f_{S(t)}(s)$.

Fig. 2 shows the time-averaged ccdf for various values of M and α, each of them computed with the presented approach.[4] Additionally, the results of Monte–Carlo simulations are depicted. As one can see, the numerically calculated curves are well in accordance with the ones obtained by simulation.

Fig. 3 compares the (time-averaged) iccdf (probability $\psi = 10^{-5}$) for different cardinalities M over the roll-off factor α. As already supposed on the basis of approximations

[2] By choosing $K = 2000$, we can ensure that—even in the case of $\alpha = 0$ (ideal low-pass filter)—more than 99.99 percent of the pulse shape's total energy are gathered. In [12], it was shown that 99.9 percent of total energy are enough, so that further increases of K do not have relevant impacts on the distribution of instantaneous power.

[3] In case of a symmetric impulse response $g(t)$, as stated in [7], one take advantage of the statistic properties' symmetry wrt. $t = T/2$.

[4] The characteristic functions were represented by 2^{21} samples within the interval $s \in (-32, 32]$ (here: s dimensionless quantity) in order to minimize effects that are associated with the FFT (leakage, cyclic convolution). The integral in (7) was evaluated numerically using equidistant ($\Delta t = T/\beta$ with $\beta = 128$) sampling, i.e., β different distributions have been averaged, cf. [7], [12].

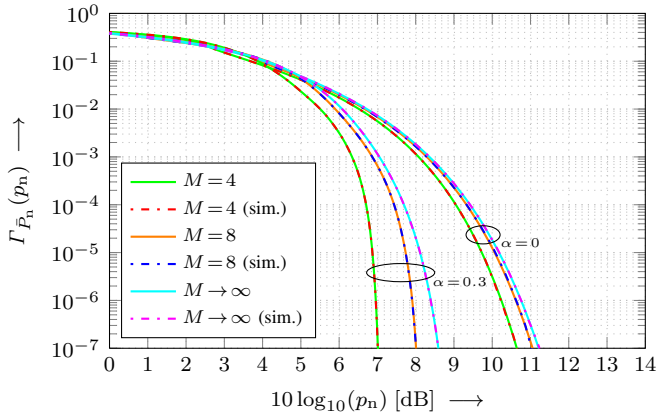

Fig. 2. Time-averaged ccdf of the normalized instantaneous power for ASK obtained by numerical calculation using FFT. For comparison, the results from Monte–Carlo simulation are shown.

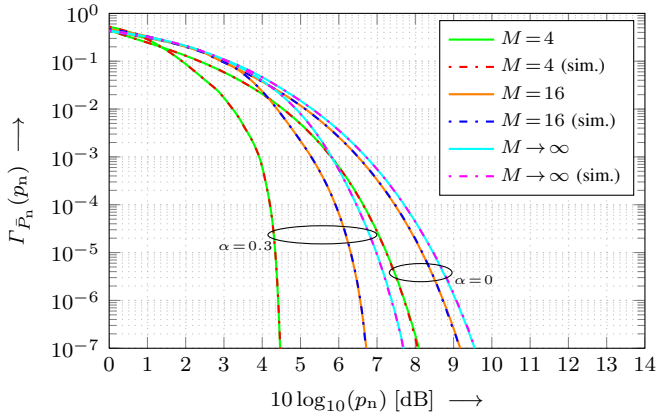

Fig. 4. Time-averaged ccdf of the normalized instantaneous power for QAM obtained by numerical calculation using FFT. For comparison, the results from Monte–Carlo simulation are shown.

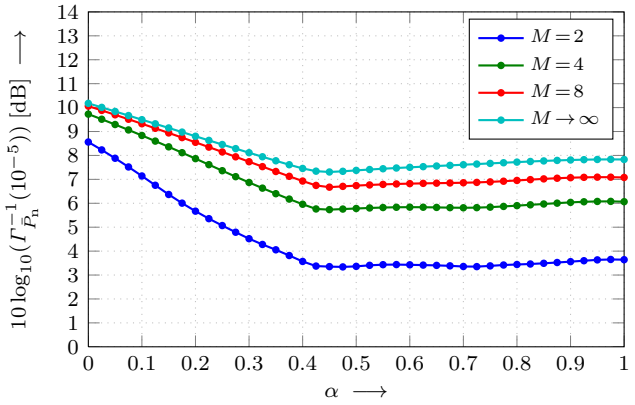

Fig. 3. Time-averaged iccdf of the normalized instantaneous power for ASK over the roll-off factor α of the basic pulse $g(t)$.

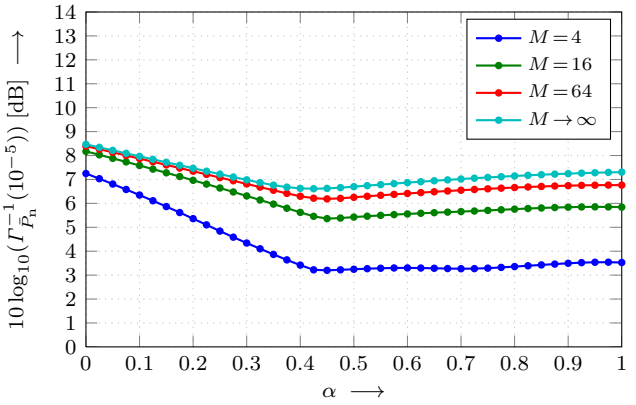

Fig. 5. Time-averaged iccdf of the normalized instantaneous power for QAM over the roll-off factor α of the basic pulse $g(t)$.

or simulations in [12], the PAR behavior gets worse with increasing cardinality of the signal constellation. However, the influence of the roll-off factor is not monotonous—best performance is achieved for α between 0.4 and 0.5. This effect is caused as the characteristics of the cyclostationarity change with α. A detailed discussion is given in Section IV.

D. Extension to QAM

The strategy presented in the previous section can easily be extended to square QAM constellations, where real and imaginary part are drawn independently. If $g(t)$ is real valued, the ECB transmit signal can be written as $S(t)=S_\mathrm{I}(t)+\mathrm{j}\,S_\mathrm{Q}(t)$, each quadrature component originating from the coefficients $A_\mathrm{I}[k]$ and $A_\mathrm{Q}[k]$, respectively. Since $f_{S_\mathrm{I}(t)}(s)=f_{S_\mathrm{Q}(t)}(s)\overset{\text{def}}{=}f_{S_\times(t)}(s)$, the corresponding characteristic function reads

$$\varphi_{S_\times(t)}(\omega)=\prod_{\kappa=1}^{K}\left(\frac{2}{\sqrt{M}}\sum_{m=1}^{\sqrt{M}/2}\cos(\omega g_\kappa(t)a_m c_\mathrm{QAM})\right), \tag{14}$$

or in the case of $M\to\infty$ as

$$\varphi_{S_\times(t)}(\omega)=\prod_{\kappa=1}^{K}\mathrm{si}(\omega g_\kappa(t)\sqrt{3/2})\,. \tag{15}$$

Due to independence, the characteristic function of $P(t)=S_\mathrm{I}^2(t)+S_\mathrm{Q}^2(t)$ is obtained by

$$\varphi_{P(t)}(\omega)=\left(\varphi_{S^2_\times(t)}(\omega)\right)^2\,. \tag{16}$$

Hence, after Fourier transform, normalization and time averaging are performed just like in the real-valued case to obtain the requested average pdf of the normalized instantaneous power.[5]

Fig. 4 compares the numerical results[6] for the time-averaged ccdf with that obtained from numerical simulations. For all

[5]Although the numerical calculation of $\varphi_{S_\times(t)}(\omega)$ does not differ from the one-dimensional case in principle, the present approach raises the problem of obtaining the characteristic function $\varphi_{S^2_\times(t)}(\omega)$ from $\varphi_{S_\times(t)}(\omega)$. Unfortunately, this cannot be done directly. Instead, we first have to compute the pdf $f_{S_\times(t)}(s)$ via FFT. As a discrete representation of $f_{S^2_\times(t)}(p)$ with equidistant samples is desired, each sample of $f_{S_\times(t)}(s)$ is mapped to the corresponding nearest position $p=s^2$ of $f_{S^2_\times(t)}(p)$. Even though this is a lossy (quantized) transformation, the inaccuracies are negligible if a large amount of samples is used. Once we have obtained $f_{S^2_\times(t)}(p)$, the desired pdf $f_{P(t)}(p)$ can be computed via fast convolution, which is an efficient (FFT-based) practical implementation of (16).

[6]Here, $f_{S_\times(t)}(s)$ was represented via 2^{19} samples within $s\in[-16,16]$ and $f_{S^2_\times(t)}(p)$ via 2^{21} samples within $p\in[0,64]$. $\beta=128$ time positions were used.

values of the parameters α and M, the theoretical curves match very well with the results of Monte–Carlo simulations.

Fig. 5 shows the iccdf (probability $\psi = 10^{-5}$) for different cardinalities M over the roll-off factor α. For QAM, the same characteristics as in the case of ASK transmission are present. However, in general, a somewhat better behavior of the PAR can be observed.

III. Multi-Carrier Signals

A. System Model

In this section, we consider multi-carrier transmission via OFDM. The assumed system model is depicted in Fig. 6.

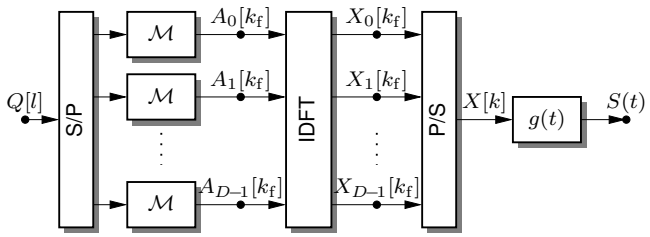

Fig. 6. Transmitter model of OFDM multi-carrier transmission.

The redundancy-free sequence of source symbols is demultiplexed into D parallel bitstreams by serial-to-parallel conversion. Each is mapped to signal points drawn from the same constellation $\mathcal{A}$, forming a *frame* of symbols $\boldsymbol{A}[k_\mathrm{f}] \stackrel{\mathrm{def}}{=} [A_0[k_\mathrm{f}], \ldots, A_{D-1}[k_\mathrm{f}]]$ in frequency domain, where k_f denotes the frame index. The frame $\boldsymbol{X}[k_\mathrm{f}] \stackrel{\mathrm{def}}{=} [X_0[k_\mathrm{f}], \ldots, X_{D-1}[k_\mathrm{f}]]$ of corresponding time-domain symbols is calculated using an inverse discrete Fourier transform (IDFT)

$$X_l[k_\mathrm{f}] = \frac{1}{\sqrt{D}} \sum_{j=0}^{D-1} A_j[k_\mathrm{f}] \cdot \mathrm{e}^{\mathrm{j}\frac{2\pi}{D} jl}\,, \quad l \in \{0, \ldots, D-1\}\,. \tag{17}$$

Via parallel-to-serial-conversion, a sequence of (complex-valued) time-domain symbols $X[k]$ is obtained, which constitute the amplitude coefficients for RRC pulse shaping according to (1) to generate the continuous-time ECB transmit signal $S(t)$. Hence, for the generation of the transmit signal, OFDM can simply be seen as single-carrier transmission, where the amplitude coefficients are not directly drawn from a QAM alphabet but are generated by some means of preprocessing. As usual in the literature, the OFDM guard interval [1] is neglected in the subsequent analysis.

B. Efficient Assessment of Distributions for OFDM

For the moment, we assume that all elements of the frame $\boldsymbol{A}[k_\mathrm{f}]$ are independently drawn from the same (square) QAM constellation (independent real and imaginary part) with zero mean and variance $\sigma_A^2 = 1$. Hence, the (stationary) discrete-time process $X[k]$ possesses a constant power spectral density (PSD) $\Phi_{XX}(\mathrm{e}^{\mathrm{j}2\pi fT})$, which corresponds to uncorrelated samples in time-domain (all of them with uncorrelated real and imaginary parts [10]). As a consequence—and exactly the same as in case of single-carrier PAM transmissions—the average PSD $\bar{\Phi}_{SS}(f)$ of the process $S(t)$ is simply proportional to the energy spectrum $|G(f)|^2$ of the basic pulse shape. This fact is illustrated in the top plot of Fig. 7.

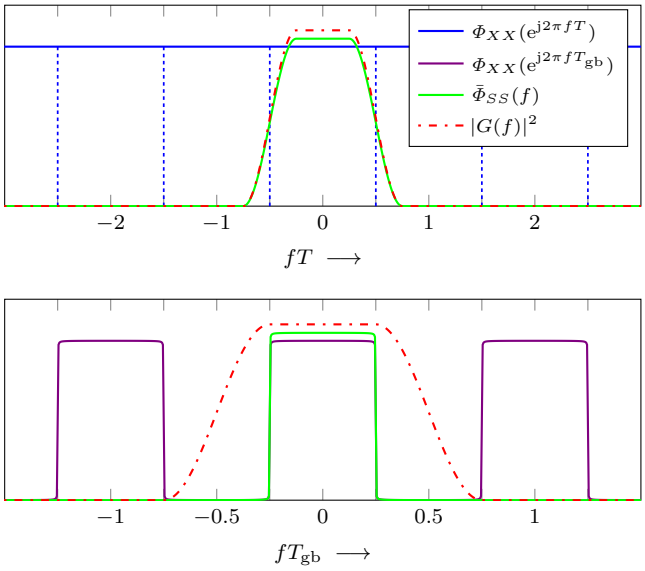

Fig. 7. Visualization of the power spectral densities of single-carrier PAM transmission and OFDM transmission without/with guard bands. Top: PSD of processes $X[k]$ and $S(t)$ for OFDM transmissions without guard bands, identical to single-carrier PAM transmissions (where $X[k] = A[k]$). RRC pulse shape with roll-off factor $\alpha = 0.5$. Bottom: PSD of processes $X[k]$ and $S(t)$ for OFDM transmissions with guard bands (oversampling, here by a factor of $D/D_\mathrm{u} = 2$). RRC pulse shape with $\alpha = 0.5$ (relative to T_gb).

Even though single- and multi-carrier modulation may possess the same PSD, the pdfs of the transmit symbols differ significantly. Due to the addition of independent, identically distributed random variables in (17), according to the central limit theorem [8], for typical numbers of subcarriers (e.g., $D \geq 128$) the distribution of the time-domain symbols $X[k]$ (at the input of the transmit filter) is well approximated by a complex Gaussian distribution [11].

Since, in the case of Gaussian distributions, uncorrelated random variables are equivalent to independent variables, the time-domain samples are (well approximated to be) independent, each with independent components. Hence, for assessing the peak-power behavior, OFDM can be simply regarded as single-carrier modulation with (complex-valued) Gaussian amplitude coefficients. As a result, $|S(t)|$ is Rayleigh distributed [8] with the filter-dependent scale parameter $\sigma_\mathrm{r}^2 = 1/2 \cdot \sum_{\kappa=1}^{K} g_\kappa^2(t)$, which gives the variance of $S_\mathrm{I}(t)$ and $S_\mathrm{Q}(t)$ at a particular time instant. Consequently, $P(t)$ is exponentially distributed (cf. [5]) and its ccdf is given as

$$\Gamma_{P(t)}(p) = \exp\left(-\frac{p}{2\,\sigma_\mathrm{r}^2}\right) = \exp\left(-\frac{p}{\sum_{\kappa=1}^{K} g_\kappa^2(t)}\right)\,. \tag{18}$$

In this way, the PAR behavior of OFDM transmissions can efficiently be approximated by an analytical expression. Fig. 8 shows the time-averaged ccdf curves that were obtained by evaluating (18). Additionally, (except for $\alpha = 0$; the curve

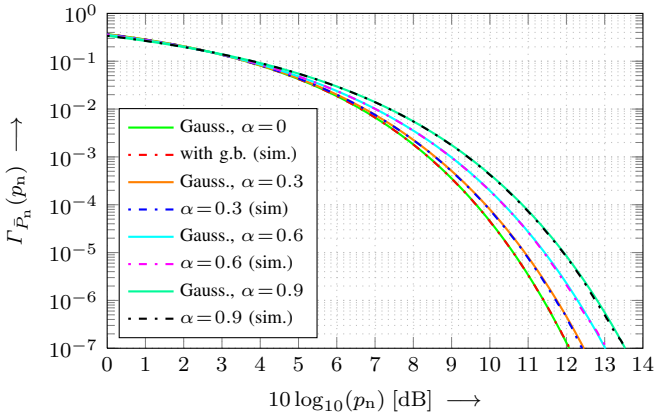

Fig. 8. Time-averaged ccdf of normalized instantaneous power of OFDM transmission for complex-valued Gaussian coefficients (analytic solution) and Monte–Carlo simulations.

labeled "with g.b." will be explained subsequently) numerical results from Monte–Carlo simulations of OFDM with $D = 512$ and 16QAM symbols are shown. On the one hand, the perfect match between simulations and approximation can be seen. On the other hand, the impact of the roll-off factor α is surprising: contrary to single-carrier transmission, the PAR gets worse when increasing α. This effect is caused by different manifestations of the cyclostationarity of the transmit signal; it will be explained in detail in Section IV.

C. Influence of Guard Bands

It is common practice, that some of the available OFDM subcarriers (i.e., modulation symbols within the frame $\boldsymbol{A}[k_\mathrm{f}]$) are not used for information transmission. Instead, several carriers (typically at the highest and/or lowest frequencies) are set to zero in order to form so-called *guard bands* [1]. We denote the number of carriers used for data transmission by D_u.

Obviously, in order to achieve the same data rate as in case of no guard bands, the symbol interval used in pulse shaping has to be shortened to $T_\mathrm{gb} \stackrel{\mathrm{def}}{=} D_\mathrm{u}/D \cdot T$. This approach can be considered as *oversampling* (D/D_u is the oversampling factor), since the frames are padded with zeros, meaning that the periodic repetitions are shifted to higher frequencies.[7] As a result, the PSD $\Phi_{XX}(\mathrm{e}^{\mathrm{j}2\pi f T_\mathrm{gb}})$ periodically exhibits band where it is (nearly) zero, as shown in the bottom plot of Fig. 7

As a consequence, even by employing a pulse shape with $\alpha \gg 0$ (relative to the interval T_gb), an almost rectangular average PSD $\bar{\Phi}_{SS}(f)$ of the transmit signal is obtained. This, however, corresponds to a (nearly) *wide-sense stationary signal* $S(t)$. Thus, in strong contrast to OFDM transmissions without guard bands or single-carrier PAM, the basic pulse shape has (almost) no impact on the PSD as long as it suppresses the periodic repetitions and exhibits a constant transfer function in the range of the used subcarriers.

[7]When using $D_\mathrm{u} = 512$ out of $D = 1024$ carriers and hence $T_\mathrm{gb} = T/2$, the periodic repetitions only appear at $f = v \cdot 2/T$, $v \in \mathbb{Z}$.

The influence of the guard bands and the associated wide-sense stationarity of the transmit signal is demonstrated by Monte–Carlo simulation (16QAM symbols) for $D = 1024$, $D_\mathrm{u} = 512$ and RRC pulse shape with $\alpha = 0.5$ (relative to T_gb). For this setting, an almost rectangular PSD $\bar{\Phi}_{SS}(f)$ is achieved. As can be seen from Fig. 8 (labeled "with g.b."), as expected from the theoretical considerations, the ccdf coincides with that for Gaussian coefficients and ideal low-pass filtering. Thus, the use of guard bands, which naturally leads to a wide-sense stationary transmit signal, even has a positive effect on the PAR of OFDM.

IV. Comparison of Single- and Multi-Carrier Signals

In this section, we compare the PAR behavior of single- and multi-carrier modulated signals. In addition, we provide an explanation for the contradictory influence of the roll-off factor on both modulation techniques. To this end, Fig. 9 shows the iccdf (probability $\psi = 10^{-5}$) for the single- (QAM modulation) and multi-carrier (OFDM) case. By computing the iccdf for the individual time instances $t = 0$ and $t = T/2$, as well as the time-averaged icddf, the impact of the cyclostationarity of the transmit signal can be grasped.

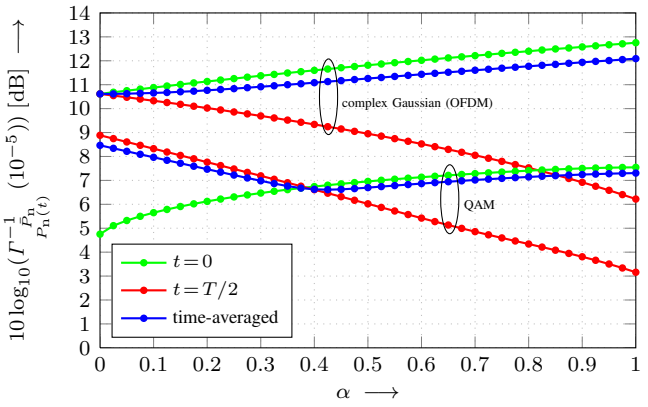

Fig. 9. Iccdf of normalized instantaneous power for observation times $t = 0$ and $t = T/2$ together with the time-averaged result. Single-carrier transmission using QAM (here: $M \to \infty$) and multi-carrier transmission (OFDM).

Considering the Gaussian distribution of the coefficients $X[k]$ in OFDM (without guard bands), the explanation for the degrading PAR behavior when increasing α is straightforward: Since the Gaussian pdf remains Gaussian in case of convolution [8], the transmit signal $S(t)$ obtained from pulse shaping is also Gaussian. In the wide-sense stationary case ($\alpha = 0$), the same (complex) Gaussian distribution is present at any observation time $t \in [0, T)$ as i) the average power[8] (ensemble average) does not vary over time and ii) a zero-mean Gaussian distribution is completely defined by its variance. Hence, the ccdf of the normalized instantaneous power is identical to the time-averaged one and reads $\Gamma_{\bar{P}_\mathrm{n}}(p_\mathrm{n}) = \mathrm{e}^{-p_\mathrm{n}}$.

[8]As we consider only zero-mean processes, the average power coincides with the variance.

However, the variance (ensemble average) of the transmit signal $S(t)$, which is determined by the sum of squared filter coefficients at a given observation time (cf. (18)), shows an increasing fluctuation over the symbol interval if α is increased. In particular, the variance around $t = T/2$ decreases (and hence does the iccdf curve), whereas the variance around $t = 0$ (and the iccdf curve) increases over α. As the time-averaged PAR behavior is dominated by the worst-case distribution within one symbol duration, it gets worse when increasing α. In summary, we can conclude that the use of guard bands (oversampling) in OFDM results in a (wide-sense) stationary transmit signal and, in turn, in the best possible PAR.

In contrast, in the single-carrier case, uniformly distributed amplitude coefficients $A[k]$ lead, after pulse shaping, to a transmit signal $S(t)$, which exhibits a distribution that completely differs from a Gaussian one. Although the variance (ensemble average) does not vary over time for $\alpha = 0$, the distributions of various observation instances significantly differ as higher moments [8] are relevant, too.

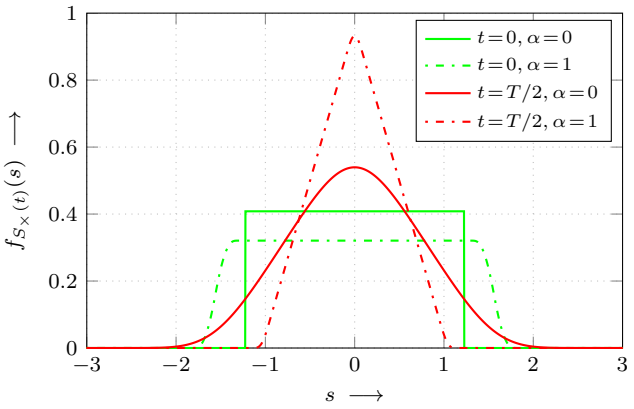

Fig. 10. Pdf of $S_\times(t)$ ($M \to \infty$) in case of $\alpha = 0$ (wide-sense stationary transmit signal) and $\alpha = 1$ (maximum variations over time).

This property is illustrated in Fig. 10, where the pdf of $S_\times(t)$ (QAM constellation with $M \to \infty$) is shown for $t = 0$ and $t = T/2$ and an RRC pulse with roll-off factor $\alpha = 0$ and $\alpha = 1$. As one can see, the distribution at $t = T/2$ dominates the PAR behavior for $\alpha = 0$. By increasing the roll-off factor to $\alpha = 1$, we can improve the situation around $t = T/2$, as the average power at this time instance is decreased. However, this comes at the cost of the distribution at $t = 0$, where the average power increases. Consequently, considering Fig. 9, the distributions around $t = T/2$ are the dominating contributions for $\alpha < 0.4$. For approximately $\alpha > 0.4$, the distributions around $t = 0$ are dominating.

As can bee seen from Fig. 9, in general, OFDM transmission shows an inferior PAR. However, to obtain a fair comparison which is relevant in practice, the OFDM guard bands have to be taken into account. This, in turn, leads to a comparison of different spectral shapes, as shown in Fig. 7. Hence, to be fair, OFDM transmission (with guard bands) has to be compared to single-carrier transmissions with (nearly) ideal low-pass filtering. Only in this case, the PSDs of the respective transmit signals are identical. Assuming a QAM constellation of large cardinality for single-carrier transmission, for $\alpha = 0$ only a difference of about 2 dB is left (probability $\psi = 10^{-5}$). This final gap reflects the difference between Gaussian and uniform distributed amplitude coefficients and vanishes if signal shaping [3] is used.

V. Conclusion

In this paper, we have presented a new approach for the assessment of instantaneous power distributions of single-carrier PAM transmissions based on characteristic functions. An efficient and accurate FFT-based numerical implementation was given. Besides this, the suitability of the Gaussian approximation for OFDM multi-carrier transmission has been reviewed. The positive influence of guard bands on the PAR behavior has been worked out. Moreover, the converse impact of cyclostationarity on single- and multi-carrier signals has been discussed. A fair comparison of both modulation techniques (same shape of the PSD) reveals that the respective PAR distributions are much more similar than often stated.

References

[1] J.A.C. Bingham. Multicarrier Modulation for Data Transmission: An Idea Whose Time Has Come. *IEEE Communications Magazine*, vol. 28, no. 5, pp. 5–14, May 1990.

[2] S. Daumont, B. Rihawi, Y. Lout. Root-Raised Cosine Filter Influences on PAPR Distribution of Single Carrier Signals. *Proceedings of 3rd International Symposium on Communications, Control and Signal Processing (ISCCSP)*, pp. 841–845, Mar. 2008.

[3] R.F.H. Fischer. *Precoding and Signal Shaping for Digital Transmission*. John Wiley & Sons, New York, 2002.

[4] W.A. Gardner, L. Franks. Characterization of Cyclostationary Random Signal Processes. *IEEE Transactions on Information Theory*, vol. 21, no. 1, pp. 4–14, Jan. 1975.

[5] S. Müller, R. Bäuml, R.F.H. Fischer, J.B. Huber. OFDM with Reduced Peak-to-Average Power Ratio by Multiple Signal Representation. *Annals of Telecommunications*, vol. 52, no. 1–2, pp. 58–67, Feb. 1997.

[6] H. Ochiai, H. Imai. On the Distribution of the Peak-to-Average Power Ratio in OFDM Signals. *IEEE Transactions on Communications*, vol. 49, no. 2, pp. 282–289, Feb. 2001.

[7] H. Ochiai. Exact and Approximate Distributions of Instantaneous Power for Pulse-Shaped Single-Carrier Signals. *IEEE Transactions on Wireless Communications*, vol. 10, no. 2, pp. 682–692, Feb. 2011.

[8] A. Papoulis, S.U. Pillai. *Probability, Random Variables and Stochastic Processes*. Fourth Edition, McGraw-Hill, New York, 2002.

[9] J.G. Proakis, M. Salehi. *Digital Communications*. Fifth Edition, McGraw-Hill, New York, 2007.

[10] S. Shepherd, J. Orriss, S. Barton. Asymptotic Limits in Peak Envelope Power Reduction by Redundant Coding in Orthogonal Frequency-Division Multiplex Modulation. *IEEE Transactions on Communications*, vol. 46, no. 1, pp. 5–10, Jan. 1998.

[11] C. Siegl. *Peak-to-average Power Ratio Reduction in Multi-antenna OFDM Via Multiple Signal Representation*. PhD Thesis, University Erlangen, 2010.

[12] M. Tanahashi, H. Ochiai. On the Distribution of Instantenous Power in Single-Carrier Signals. *IEEE Transactions on Wireless Communications*, vol. 9, no. 3, pp. 1207–1215, Mar. 2010.

[13] D. Wulich, L. Goldfeld. Bound of the Distribution of Instantaneous Power in Single Carrier Modulation. *IEEE Transactions on Wireless Communications*, vol. 4, no. 4, pp. 1773–1778, July 2005.

[14] G. Wunder, H. Boche. Upper Bounds on the Statistical Distribution of the Crest-Factor in OFDM Transmission. *IEEE Transactions on Information Theory*, vol. 49, no. 2, pp. 488–494, Feb. 2003.